FFT-based Computation of the Bioheat Transfer Equation for the HCC Ultrasound Surgery Therapy Modeling

Jean-Louis Dillenseger, Simon Esneault and Carole Garnier

***Abstract*— This paper describes a modeling method of the tissue temperature evolution over time in hyperthermia. More precisely, this approach is used to simulate the hepatocellular carcinoma curative treatment by a percutaneous high intensity ultrasound surgery. The tissue temperature evolution over time is classically described by Pennes' bioheat transfer equation which is generally solved by a finite difference method. In this paper we will present a method where the bioheat transfer equation can be algebraically solved after a Fourier transformation over the space coordinates. The implementation and boundary conditions of this method will be shown and compared with the finite difference method.**

I. INTRODUCTION

At an early stage, the hepatocellular carcinoma (HCC) is commonly confined to a solitary mass which is potentially curable by a percutaneous surgical resection such as percutaneous ethanol injection, or radiofrequency ablation [1]. Ultrasound surgery are now proposed within this interstitial applicators context [2]. The therapeutic ultrasound device is composed of a small (3 mm x 10 mm) planar ultrasonic mono-element transducer encapsulated in a $\varnothing$ 4 mm cylindrical interstitial applicator which is set within the tumor under ultrasound image guidance. The therapy consists in a sequence of exposures. After each exposure the applicator can be rotated by a specific angle in order to deposit heat according to the tumor geometry. This method offers the advantage to be more controllable in depth and direction than other interstitial heating modalities. Like any other minimally invasive image guided therapy, its clinical application requires an efficient planning at the pre-operative stage. This paper will deal with the design of a physically-based model of the delivered thermal dose.

The framework of the modeling involves to compute 1) the tissue temperature T evolution over time and then 2) to estimate the thermal damages (the necrotic volume) induced by the heating [3], [4].

1) Classically in hyperthermia, the tissue temperature T evolution over time is obtained by solving Pennes' bioheat transfer equation (BHTE) [5]:

$$\rho_t C_t \frac{\partial T}{\partial t} = k_t \nabla^2 T + V \rho_b C_b (T_b - T) + Q \qquad (1)$$

where: ρ_t and C_t refer to tissue density and specific heat; $k_t \nabla^2 T$ models the thermal diffusion with k_t the thermal conductivity of tissue; $V \rho_b C_b (T_b - T)$ models the effect of perfusion where V, ρ_b, C_b and T_b are respectively the perfusion rate per unit volume of tissues, the density, the specific heat and the temperature of blood; and Q the rate of the heat per unit volume of tissue produced by the source.
In the case of high intensity ultrasound therapy, Q is an acoustical power given by $Q = \beta f p^2 / \rho_t c$ where β is the absorbtion coefficient of ultrasound in tissues which depends on the tissue temperature [6]; f, the ultrasound frequency; c, the ultrasound velocity and p, the pressure delivered by the ultrasound device which depends on the physical and the tissue assumptions [7].

2) The concept of thermal dose [8] is used to assess thermal damages. For each location and history of temperature, the thermal dose is defined as an equivalent time the temperature of reference of $43°\mathrm{C}$ should be applied to obtain the same thermal damage. It can be computed directly from the temperature map:

$$D_{43°\mathrm{C}}(x,y,z,t) = \sum_{i=1}^{t} R^{(43-T(x,y,z,t))} \Delta t \qquad (2)$$

with $R = 0.5$ if $T > 43°\mathrm{C}$ and $R = 0.25$ otherwise. Liver tissues are considered as irreversibly thermally damaged when $D_{43°\mathrm{C}} > 340$ minutes [9].

The BHTE (1) is generally solved by finite difference [10] or finite elements methods. A previous study (in 2D) has shown that in the case of non perfused tissues ($V = 0$) the partial equation in time can be explicitly solved in the spatial frequency space [11]. But the liver is one of the most vascularized human tissue so perfusion can no more be considered as negligible. In this paper we will extend this idea to solve the BHTE in the spatial frequency space in 3D with perfusion and combine it to the 3D modeling of the thermal coagulation necrosis induced by an interstitial ultrasonic transducer in the liver [4].

II. METHODS

A. BHTE solving

If we consider that the coefficients ρ_t, C_t, k_t, V, ρ_b, and C_b remain constant over time, then (1) can be rewritten as:

$$A \frac{\partial T(\mathbf{x},t)}{\partial t} = B \nabla^2 T(\mathbf{x},t) + C(T_b(\mathbf{x}) - T(\mathbf{x},t)) + Q(\mathbf{x},t) \qquad (3)$$

This work is part of the national SUTI project supported by an ANR Grant (ANR05RNTS01106).

J.-L. Dillenseger, S. Esneault and C. Garnier are with INSERM, U642, Rennes, F-35000, France; and with Université de Rennes 1, LTSI, Rennes, F-35000, France {jean-louis.dillenseger, simon.esneault, carole.garnier}@univ-rennes1.fr

where: $\mathbf{x}$ is the spatial coordinates, t the time parameter, $A = \rho_t C_t$, $B = k_t$ and $C = V\rho_b C_b$.

If we take the Fourier transformation of (3) over the space coordinates and use the property that if $F(\mathbf{x})$ is a differentiable function with Fourier transform $F^*(\mathbf{v})$ (where the symbol * denotes the Fourier Transform and $\mathbf{v}$ the spatial frequency coordinates), then the Fourier transform of its derivative is given by $j2\pi\mathbf{v}F^*(\mathbf{v})$, so:

$$A\frac{\partial T^*(\mathbf{v},t)}{\partial t} = -4\pi^2\mathbf{v}^2 BT^*(\mathbf{v},t) + C(T_b^*(\mathbf{v}) - T^*(\mathbf{v},t)) + Q^*(\mathbf{v},t) \quad (4)$$

The second order partial differential equation over the space domain is translated into an algebraic equation.

If we consider that the acoustic power $Q(\mathbf{x},t)$ remains constant over time, (4) can be rewritten as a first-order differential equation over the time:

$$A\frac{\partial T^*(\mathbf{v},t)}{\partial t} + (4\pi^2\mathbf{v}^2 B + C)T^*(\mathbf{v},t) = CT_b^*(\mathbf{v}) + Q^*(\mathbf{v}) \quad (5)$$

If $T_{init}^*(\mathbf{v})$ is the Fourier transform of the initial temperature map at $t = 0$, an analytical solution can be found for (5):

$$T^*(\mathbf{v},t) = T_{init}^*(\mathbf{v})\exp^{-\frac{(4\pi^2\mathbf{v}^2B+C)t}{A}} + \frac{CT_b^*(\mathbf{v}) + Q^*(\mathbf{v})}{4\pi^2\mathbf{v}^2B + C}\left(1 - \exp^{-\frac{(4\pi^2\mathbf{v}^2B+C)t}{A}}\right) \quad (6)$$

B. Implementation and boundary conditions

Some properties of the ultrasound therapy and boundary conditions must be taken into account for the implementation:

- The thermal dose (2) is an integration. The temperature must be computed at several time steps Δt.
- The front transducer face is cooled by a continuous flow of degassed water maintained at a constant temperature. The temperature of the cooling water serves as an isothermal boundary condition. But this condition cannot be described explicitly in (6). However, this condition can be incorporate in the model by the following iterative process:
  1) With (6), compute explicitly $T(\mathbf{x},\Delta t)$, the temperature map at a specific time step Δt.
  2) In $T(\mathbf{x},\Delta t)$, modify the temperature for the $\mathbf{x}$ within the interstitial ultrasonic transducer to the temperature of the cooling water.
  3) The modified $T(\mathbf{x},\Delta t)$ serves then as a new initial temperature $T_{init}(\mathbf{x})$ map for (6) in order to compute the temperature map at the next time step Δt.
- As ebullition is not considered in the present model and for avoiding unrealistic temperatures; a threshold must ensure that the temperature could never exceed $100°\mathrm{C}$. This threshold is incorporated in the model using the iterative process described previously.
- In [4], [7], we have shown that for more realistic modeling, the acoustic power Q is temperature dependent and so does not remain constant over time. However, because the temperature evolution over time is relatively slow, we can consider that Q remains constant during a time step Δt. So Q needs only to be actualized after each Δt and can be incorporated in the model using the iterative process described previously.

The implemented algorithm can so be summarized by:

1) Initialization. $T_b(\mathbf{x})$ is build by setting the temperature within the interstitial ultrasonic transducer to the temperature of the cooling water and to $37°\mathrm{C}$ elsewhere. $T_b^*(\mathbf{v})$ is then computed. At $t = 0$, $T_{init}^*(\mathbf{v})$ is set the same as $T_b^*(\mathbf{v})$. $Q(\mathbf{x})$ and so $Q^*(\mathbf{v})$ are also computed at $t = 0$.
2) Temperature map estimation. At $t = t+\Delta t$, $T^*(\mathbf{v},\Delta t)$ is computed using (6) in order to estimate $T(\mathbf{x},\Delta t)$.
3) Boundary effects and thermal dose. $T(\mathbf{x},\Delta t)$ is modified in order to take the cooling water effect and temperature threshold into account. The thermal dose (2) is updated.
4) Acoustical power. $Q(\mathbf{x})$ can be computed by taking new shooting parameters and/or the new temperature map $T(\mathbf{x},\Delta t)$ into account.
5) Next iteration initialization. The new $T_{init}^*(\mathbf{v})$ is estimated from the Fourier Transform of $T(\mathbf{x},\Delta t)$ modified at step 3. The new $Q^*(\mathbf{v})$ is also computed. t is incremented by Δt and a new iteration can be computed from step 2.

III. Results and Discussion

A. Simulation context

For evaluation purpose, we choose to simulate a real in-vivo experiment described in [2]. A 10.7 MHz therapeutic ultrasound was positioned inside the liver of pigs, away from large blood vessels. This animal experimentation was approved by a veterinarian ethics committee. The exposure conditions were set to: $14\ \mathrm{W/cm^2}$ for the intensity measured by a force balance at the surface of the applicator; $37°\mathrm{C}$ for the transducer cooling water temperature and 20 s for the duration of the exposure. Four thermocouples were introduced inside liver on the acoustic axis of the transducer right at the end of the 20 s-long exposure. The maximum increase of temperature was measured at four different positions: 2.5, 5, 7.5 and 10 mm from the applicator surface.

B. Method implementation

The simulation is performed within a $201 \times 201 \times 61$ volume grid with a sampling step $\Delta\mathbf{x}$ of 0.4 mm on each direction (which corresponds to a simulation volume of size $80\ \mathrm{mm} \times 80\ \mathrm{mm} \times 24\ \mathrm{mm}$). The simulated applicator is set in the middle of this volume. Fourier transforms were computed using the classical 3D FFT algorithm computed on a $256 \times 256 \times 64$ elements volume grid. The used tissue acoustical and thermal properties were found in the

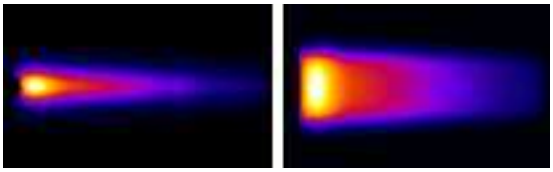

Fig. 1. Simulated temperature maps. Left: cut plane perpendicular to the applicator axis. Right: cut plane along the applicator axis. The temperature color scale goes from black (37°C) to white (66°C).

Fig. 2. Simulated necrotic volume. Left: cut plane perpendicular to the applicator axis. Right: cut plane along the applicator axis.

literature [12], [13], [14] and set to: $\rho_t = 1050\ \mathrm{kg \cdot m^{-3}}$, $C_t = 3639\ \mathrm{J \cdot kg^{-1} \cdot^\circ C^{-1}}$, $k_t = 0.56\ \mathrm{W \cdot m^{-1} \cdot^\circ C^{-1}}$, $V\rho_b = 30\mathrm{kg \cdot m^{-3} \cdot s^{-1}}$ and $C_b = 3825\ \mathrm{J \cdot kg^{-1} \cdot^\circ C^{-1}}$. The pressure p is computed using a discrete Rayleigh integral [7] and considered as invariant over time. On the contrary, the acoustical power $Q(\mathbf{x}, t)$ is updated after each time step Δt as follows: at each spatial location $\mathbf{x}$, the absorbtion coefficient $\beta(\mathbf{x}, t)$ is estimated according to Connor's 6th order polynomial approximation of the absorbtion coefficient curve vs. temperature [6] for the temperature $T(\mathbf{x}, t)$.

As an example, Fig. 1 presents the simulated temperature maps computed at $t = 20$ s on two orthogonal cut planes (Fig. 1-left: axial cut plane perpendicular to the applicator axis; Fig. 1-right: sagittal cut plane along the applicator axis). Fig. 2 shows the corresponding simulated necrotic volumes (in white on the figure).

Fig. 3 compares the real temperatures measured on the in-vivo experimental validation at the four different positions [2] and the temperature curves obtained by our simulation method. The temperature curve obtained by our approach seems to match with the experimental data. The effect of the transducer cooling water can also be noticed near the applicator surface (on the left of the curve).

C. Time step influence

In section II-B, it has been shown that the choice of the time step Δt is crucial for the balance between computation speed and accuracy of the model. In order to evaluate the influence of Δt, several BHTEs were computed with Δt varying from 0.1 s to 20 s.

Fig. 4 presents the temperature curves along the axis perpendicular to the transducer surface and obtained when computing the BHTE with the several Δt. The curves are very similar when $\Delta t \leq 2$ s. Only the temperature profiles near the applicator surface are a bit different. This is due to the different cooling water iso-thermal boundary condition refreshment rates. However, the curves are relatively different when $\Delta t > 2$ s. In these cases, the low refreshment rate

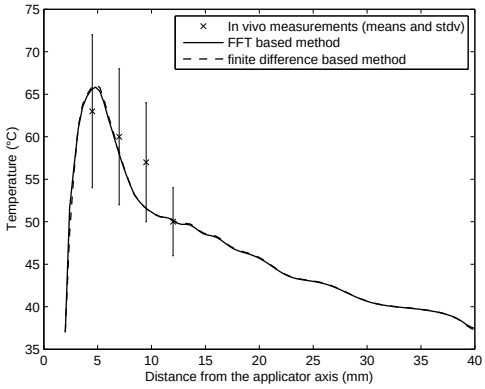

Fig. 3. Comparison between the experimental in-vivo temperature measurements and the simulated temperatures obtained with the FFT based method and the finite difference based method.

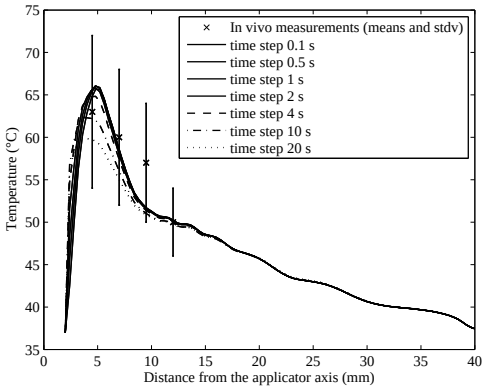

Fig. 4. Comparison between the simulated temperatures obtained with Δt varying from 0.1 s to 20 s.

TABLE I
TEMPERATURE FIELD ESTIMATION MEAN SQUARED ERRORS AND COMPUTATION TIME VS. TIME STEP

Δt (s)	0.1	0.5	1	2	4	10	20
MSE ($^\circ$C^2)	0	0.23	0.75	1.75	3.06	4.61	5.41
Comp. time (s)	1504	292	147	70	35	12	5

affects not only the cooling water iso-thermal boundary condition but also the estimation of the acoustical power Q. This is confirmed by error measurements: the curve computed with $\Delta t = 0.1$ s is considered as reference; the Mean Squared Errors between the other curves and the reference curve are reported on Table I. The computation times of the 20 s sequence simulations (computed on a conventional PC: Pentium 4 3.2 GHz proc. with 1GB RAM) are also reported on Table I.

D. Comparison with the finite difference method

The BHTE can be discretized with the finite difference scheme where the temperature $T^{n+1}(\mathbf{x})$ at step $n+1$ can be deduced from $T^n(\mathbf{x})$ by the following numerical expression [15]:

$$T^{n+1}(\mathbf{x}) = T^n(\mathbf{x}) + \frac{\delta t}{\rho_t C_t} \cdot \left(k_t \nabla^2_{discret} T^n(\mathbf{x}) + V \rho_b C_b (T_b - T^n(\mathbf{x})) + Q^n(\mathbf{x})\right) \quad (7)$$

with $\nabla^2_{discret} T^n(\mathbf{x})$, the discrete spatial Laplacian: $\nabla^2_{discret} T^n(x,y,z) = \frac{1}{\Delta \mathbf{x}^2}(T^n(x-1,y,z) + T^n(x+1,y,z) + T^n(x,y-1,z) + T^n(x,y+1,z) + T^n(x,y,z-1) + T^n(x,y,z+1) - 6T^n(x,y,z))$; $\Delta \mathbf{x}$, the spatial sampling step and δt the time sampling step which should satisfy the following inequality [15]:

$$\delta t \leq \frac{2\Delta \mathbf{x}^2 \rho_t C_t}{V \rho_b C_b \Delta \mathbf{x}^2 + 12 k_t} \quad (8)$$

In our case, $\delta t \leq 180$ ms.

The comparison framework of both BHTE solving methods is:

- the FFT-based computation method used a $\Delta t = 2$ s;
- the finite difference method used a $\delta t = 0.1$ s. Q is actualized after the same $\Delta t = 2$ s as for the FFT-based computation method.

The temperature maps obtained by both methods were almost similar (Fig. 3). More surprisingly, the computation times of both methods were also very close: 70 s and 67 s for respectively the FFT-based and the finite difference method.

Our starting hypothesis was that the BHTE algebraic solving using the FFT-based method should bring good computation time performances. However, its performance is less good as expected. This is mainly due to the FFTs which are computation time consuming: for each Δt iteration two direct FFTs ($T^*_{init}(\mathbf{v})$ and $Q^*(\mathbf{v})$) and one inverse FFT ($T(\mathbf{x}, \Delta t)$) must be computed.

In our specific case, the thermal dose integration, the cooling water iso-thermal boundary condition and the fact that the acoustical power Q is temperature dependent (and so time dependent) oblige to compute the temperature for a relatively short sampling interval of around 2 s. For this reason, the algebraically BHTE solving did not provide the expected performance. However, some gain could be obtained using specialized signal processing or mathematical libraries or vector processors in order to accelerate the Fourier Transforms computation.

At the other hand, the FFT-based method could be interesting for other hyperthermia problems or models in which the heat deposit and the boundary conditions are less dependent on the time evolution (ie. radiofrequency).

IV. Conclusion

A method simulating the tissue temperature evolution over time in high intensity ultrasound hyperthermia interstitial therapy was described. This method solves algebraically the bioheat transfer equation after a Fourier transformation over the space coordinates. However, the integrative nature of the thermal dose, the isothermal condition induced by the transducer cooling water and the temperature dependance of the acoustical power heat deposit constrained us to decompose the entire analytical temperature evolution computation into several smaller time intervals. The temperature computation at these intermediate time steps makes the FFT-based method less efficient in terms of computation time. Notwithstanding this method becomes interesting again using specialized signal processing libraries or processors or for solving hyperthermia problems with conditions less dependent on the time evolution.

References

[1] R. A. Lencioni, H. P. Allgaier, D. Cioni, M. Olschewski, P. Deibert, L. Crocetti, H. Frings, J. Laubenberger, I. Zuber, H. E. Blum, and C. Bartolozzi, "Small hepatocellular carcinoma in cirrhosis: randomized comparison of radio-frequency thermal ablation versus percutaneous ethanol injection," *Radiology*, vol. 228, no. 1, pp. 235–40, 2003.

[2] C. Lafon, J. Y. Chapelon, F. Prat, F. Gorry, J. Margonari, Y. Theillere, and D. Cathignol, "Design and preliminary results of an ultrasound applicator for interstitial thermal coagulation," *Ultrasound Med Biol*, vol. 24, no. 1, pp. 113–22, 1998.

[3] C. Lafon, F. Prat, J. Y. Chapelon, F. Gorry, J. Margonari, Y. Theillere, and D. Cathignol, "Cylindrical thermal coagulation necrosis using an interstitial applicator with a plane ultrasonic transducer: in vitro and in vivo experiments versus computer simulations," *Int J Hyperthermia*, vol. 16, no. 6, pp. 508–22, 2000.

[4] C. Garnier, C. Lafon, and J.-L. Dillenseger, "3D modeling of the thermal coagulation necrosis induced by an interstitial ultrasonic transducer," *IEEE Trans Biomed Eng*, vol. 55, no. 2, pp. 833–7, 2008.

[5] H. H. Pennes, "Analysis of tissue and arterial blood temperatures in the resting human forearm. 1948," *J Appl Physiol*, vol. 85, no. 1, pp. 5–34, 1998.

[6] C. W. Connor and K. Hynynen, "Bio-acoustic thermal lensing and nonlinear propagation in focused ultrasound surgery using large focal spots: a parametric study," *Phys Med Biol*, vol. 47, no. 11, pp. 1911–28, 2002.

[7] J.-L. Dillenseger and C. Garnier, "Acoustical power computation acceleration techniques for the planning of ultrasound therapy," in *5th IEEE International Symposium on Biomedical Imaging (ISBI'08)*, pp. 1203–1206, 2008.

[8] S. A. Sapareto and W. C. Dewey, "Thermal dose determination in cancer therapy," *Int J Radiat Oncol Biol Phys*, vol. 10, no. 6, pp. 787–800, 1984.

[9] S. J. Graham, L. Chen, M. Leitch, R. D. Peters, M. J. Bronskill, F. S. Foster, R. M. Henkelman, and D. B. Plewes, "Quantifying tissue damage due to focused ultrasound heating observed by MRI," *Magn Reson Med*, vol. 41, no. 2, pp. 321–8, 1999.

[10] J. Chato, M. Gautherie, K. Paulsen, and R. Roemer, "Fundamentals of bioheat transfer," in *Thermal dosimetry and treatment planning* (M. Gautherie, ed.), pp. 1–56, Berlin: Springer, 1990.

[11] B. Quesson, F. Vimeux, R. Salomir, J. A. de Zwart, and C. T. Moonen, "Automatic control of hyperthermic therapy based on real-time Fourier analysis of MR temperature maps," *Magn Reson Med*, vol. 47, no. 6, pp. 1065–72, 2002.

[12] F. Dunn and W. D. O'Brien, *Ultrasonic biophysics*, vol. 7 of *Benchmark papers in acoustics*. Stroudsburg (Pennsylvania): Dowden-Hutchinson & Ross Inc., 1976.

[13] Task group report of the european society for hypermermic oncology, "Treatment planning and modeling in hyperthermia," 1992.

[14] P. Bioulac-Sage, B. Le Bail, and C. Balaudaud, "Histologie du foie et des voies biliaires," in *Hépathologie clinique* (J. Benhamou, J. Bircher, N. McIntyre, M. Rizetto, and J. Rodes, eds.), pp. 12–20, Paris: Med. sciences/Flammarion, 1993.

[15] J. Wang and O. Fujiwarea, "FDTD computation of temperature rise in the human head for portable telephones," *IEEE Trans Microw Theory Tech*, vol. 47, no. 8, pp. 1528–34, 1999.